Gravity wave interactions in the stratocumulus-topped boundary layer

By A. Balakrishna, H. Fu† AND M. E O'Neill‡

1. Motivation and objectives

Stratocumulus are low-level clouds that reside within the lowest 1 km of the atmosphere and typically form over the subtropical and midlatitude oceans defining the marine boundary layer (MBL). The specific portion of the MBL that is capped by stratocumulus is referred to as the stratocumulus-topped boundary layer (STBL), as seen in Figure 1.

Stratocumulus are the most dominant cloud by coverage: in excess of 50% shield the earth's surface in the annual mean (Wood 2012). In general, low-level clouds are important drivers of earth's circulation, as they couple to the surface via turbulence and exchange momentum, heat and moisture between the surface and the global dynamical system. However, due to their prevalence, stratocumulus have a direct effect on the global radiative exchange budget. Stratocumulus reflect nearly all incident solar insolation, are ideal emitters of longwave and allow nearly complete transmission of terrestrial infrared radiation (Wood 2012; Mellado 2017), which, combined, leads to a strong, net radiative cooling effect driving enhanced turbulent activity near the cloud top.

It is clear to see that any mechanism that causes the stratocumulus deck to break up would disrupt the radiative balance leading to potential warming if sustained. Previous studies (e.g. Randall *et al.* 1984; Slingo 1990) have demonstrated that small changes in stratocumulus coverage mimic a radiative effect akin to greenhouse-gas induced warming. Furthermore, Schneider *et al.* (2019) suggested that increasing equivalent carbon dioxide concentration to levels above 1200 parts per million leads to sustained breakup of the deck; however, subsequent reductions in carbon dioxide lead to a hysteresis effect whereby clouds reform.

We are motivated to obtain a holistic understanding of factors that influence stratocumulus breakup that can help contextualize Schneider *et al.* (2019). Specifically, we seek to investigate atmospheric mechanisms that can enhance controlling parameters of stratocumulus such as cloud-top cooling via radiative or evaporative effects, wind shear and dry-air entrainment (see Mellado 2017, and references therein) and thereby promote decoupling and dispersal of the stratocumulus deck via convective instability. In this study, we hypothesize that internal gravity waves excited by local convection in the STBL could permit breakup, and our exploration to date is discussed below.

2. Numerical representation of stratocumulus

We perform moist large-eddy simulation of the STBL with Cloud Model 1 (CM 1) (Bryan & Fritsch 2002). The governing equations are as follows

† Department of Geophysical Sciences, University of Chicago
‡ Department of Physics, University of Toronto

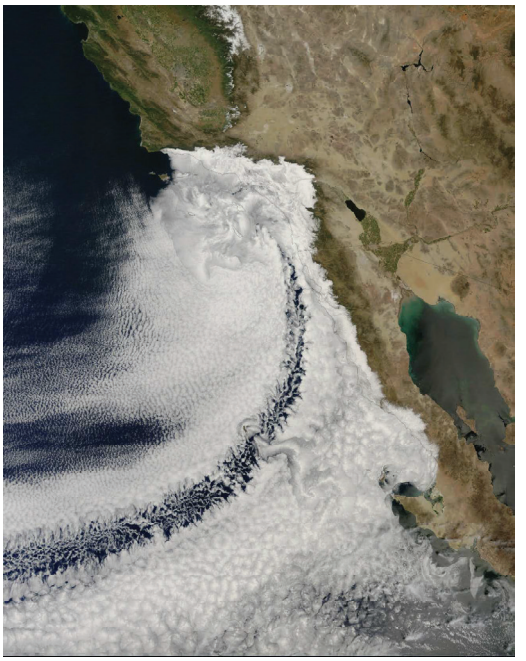

FIGURE 1. Satellite image of stratocumulus near the California Pacific coast. Image credit: NASA Earth Observing Laboratory.

$$\frac{d\pi_0}{dz} = -\frac{g}{c_p \theta_{\rho 0}}. \tag{2.1}$$

Equation 2.1 describes a moist base state that is in hydrostatic balance (i.e. only a function of the vertical coordinate, z), where $\pi = (p/p_o)^{R/c_p}$ is the Exner function and $\theta_{\rho 0}$ is the base state density potential temperature, which is a function of the potential temperature (invariant under adiabatic parcel displacement) and the specific humidities q_χ for $\chi = v, l, i$ denoting the vapor, liquid and ice phases of water. We assume that moist air behaves as an ideal gas

$$p = \rho R T (1 + q_v/\epsilon). \tag{2.2}$$

Note that $\epsilon = \mu_v/\mu_d$, the ratio of molar masses of water vapor and dry air. Mass conservation in a compressible framework stipulates

$$\frac{\partial \rho}{\partial t} + \frac{\partial}{\partial x_j}(\rho u_j) = 0 \tag{2.3}$$

and equations of motion

$$\frac{\partial u_i}{\partial t} + u_j \frac{\partial u_i}{\partial x_j} = -c_p \theta_\rho \frac{\partial \pi'}{\partial x_i} - 2\epsilon_{ijk}\Omega_j u_k + g\frac{\theta_\rho - \theta_{\rho 0}}{\theta_{\rho 0}}\delta_{i3} + \nu \frac{\partial^2 u_i}{\partial x_j \partial x_j}, \tag{2.4}$$

where primed quantities denote deviations from the base state. Next, the potential temperature and Exner function pertubations evolve according to

$$\frac{\partial \theta'}{\partial t} + u_j \frac{\partial \theta}{\partial x_j} = -\Theta_1 \theta \frac{\partial u_j}{\partial x_j} + \nu_\theta \frac{\partial^2 \theta}{\partial x_j \partial x_j} + \Theta_2(L_v \dot{q}_{cond} + L_s \dot{q}_{dep} + L_f \dot{q}_{frz}) + \Theta_3(\dot{q}_{cond} + \dot{q}_{dep}) + \dot{Q}_\theta \quad (2.5)$$

and

$$\frac{\partial \pi'}{\partial t} + u_j \frac{\partial \pi}{\partial x_j} = -\Pi_1 \pi \frac{\partial u_j}{\partial x_j} + \Pi_2(L_v \dot{q}_{cond} + L_s \dot{q}_{dep} + L_f \dot{q}_{frz}) + \Pi_3(\dot{q}_{cond} + \dot{q}_{dep}) + \Pi_4\left(\nu_\theta \frac{\partial^2 \theta}{\partial x_j \partial x_j} + \dot{Q}_\theta\right) + \Pi_5\left(\nu_{qv} \frac{\partial^2 \theta}{\partial x_j \partial x_j}\right). \quad (2.6)$$

The third and fourth terms on the right-hand side of Eqs. 2.5 and 2.6 represent latent heat effects, $\dot{Q}_\theta$ accounts for radiative warming and cooling effects from shortwave and longwave sources and Θ and Π denote constants to ensure enforcement of Eq. 2.3. Lastly, CM 1 specifies prognostic equations for q_χ

$$\frac{\partial q_v}{\partial t} + u_j \frac{\partial q_v}{\partial x_j} = \nu_{qv} \frac{\partial^2 q_v}{\partial x_j \partial x_j} - \dot{q}_{cond} - \dot{q}_{dep}, \quad (2.7)$$

$$\frac{\partial q_l}{\partial t} + u_j \frac{\partial q_l}{\partial x_j} = \nu_{ql} \frac{\partial^2 q_l}{\partial x_j \partial x_j} + \dot{q}_{cond} - \dot{q}_{frz} + \frac{1}{\rho} \frac{\partial (\rho V_l q_l)}{\partial z}, \quad (2.8)$$

and

$$\frac{\partial q_i}{\partial t} + u_j \frac{\partial q_i}{\partial x_j} = \nu_{qi} \frac{\partial^2 q_i}{\partial x_j \partial x_j} + \dot{q}_{dep} + \dot{q}_{frz} + \frac{1}{\rho} \frac{\partial (\rho V_i q_i)}{\partial z}. \quad (2.9)$$

The terms on the right-hand side of Eqs. 2.7–2.9 involving diffusion, phase change mechanisms ($\dot{q}$), precipitation, respectively, are modeled with the Morrison double-moment cloud microphysics scheme (Morrison *et al.* 2005). Note that stratocumulus are warm clouds, so $q_i = 0$ in this case.

2.1. *Solver verification*

One of the most thorough characterizations to date of the STBL was performed by Stevens *et al.* (2005). In that study, the authors performed a suite of large-eddy simulation (LES) utilizing various equation sets and phenomenological models for the subgrid scales (SGS) and microphysical effects. Quantities of interest of the stratocumulus deck, such as vertical profiles of moisture and temperature, in addition to components of the turbulent kinetic energy budget were compared against field measurements from the Dynamics and Chemistry of Marine Stratocumulus-II (DYCOMS-II) campaign (Stevens *et al.* 2003). Stevens *et al.* (2005) showed LES results nominally agree with the aircraft measurements of stratocumulus during the transient development period of the simulations within a few percent over an averaging interval of $t = [3 - 4]$ hr and displayed an approximate insensitivity to choice of model parameterizations.

Because of the relatively good agreement of Stevens *et al.* (2005) with the DYCOMS-II data, we use the same initialization based on the former and use the latter as a verification reference for CM 1. The implementation is extended from the STBL test case in CM 1.

Figure 2 illustrates the domain of interest. The sea surface acts as a wall with dynamic

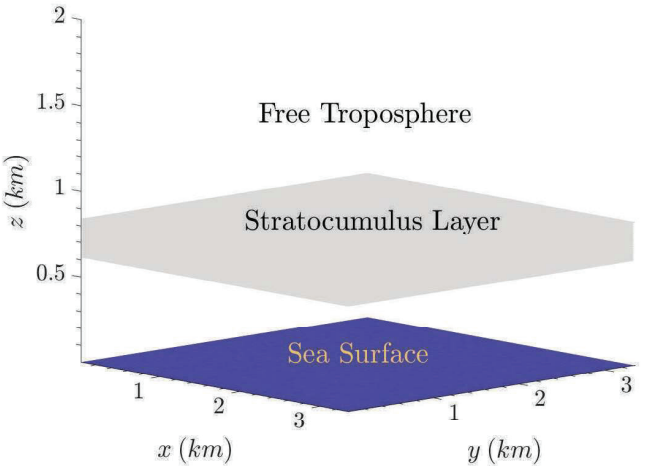

FIGURE 2. Numerical configuration of the STBL.

heat and moisture fluxes assuming a neutral stability logarithmic law (Stull 1988) with a prescribed surface roughness representative of the ocean. A constant sea surface temperature of 292.5 K is enforced. The thickness of the stratocumulus deck is quantified in regions of nonzero q_l; as mentioned previously, the region between the cloud top and ocean surface defines the boundary layer. Immediately aloft of the cloud is the (dry) free troposphere. We use a horizontal grid spacing of $\Delta x = \Delta y = 35$ m and $\Delta z = 5$ m to resolve the sharp temperature inversion (i.e. rapid change in sign of the temperature gradient) near the cloud layer in a domain of $3.4 \times 3.4 \times 1.5$ km^3. Boundary conditions are doubly periodic in-plane and partial/free-slip at the bottom/top; Rayleigh damping in the upper 100 m is utilized to prevent spurious wave reflection; and a radiation model following Stevens *et al.* (2005) is used. Lastly, note that the SGS model is the same as that described by Deardorff (1980). In terms of numerics, CM 1 utilizes a staggered grid with explicit time advancement (RK3) in the horizontal and implicit Crank–Nicholson in the vertical along with a splitting scheme to handle acoustics (Klemp & Wilhelmson 1978). A 5th order finite-difference scheme is the spatial discretization of choice to minimize excess numerical dissipation characteristic of WENO5 which is a standard choice in stratocumulus simulation (e.g. Stevens *et al.* 2005; Pressel *et al.* 2017). Figure 3 illustrates fair agreement between the CM 1 result and the DYCOMS-II data for both moisture quantities and higher order moments, though caution should be exercised that the field data are quite sparse throughout the STBL. As expected, the vicinity above the cloud layer ($z > 0.8$ km) is far dryer than within the STBL. Furthermore, since $\overline{w'w'w'}$ is proportional to the skewness of the vertical velocity, we see that $w' > 0$ is favored near the surface, which is indicative of turbulent exchange with the ocean, while a sign change in the triple correlation toward the middle of the STBL indicates favorability of downdrafts.

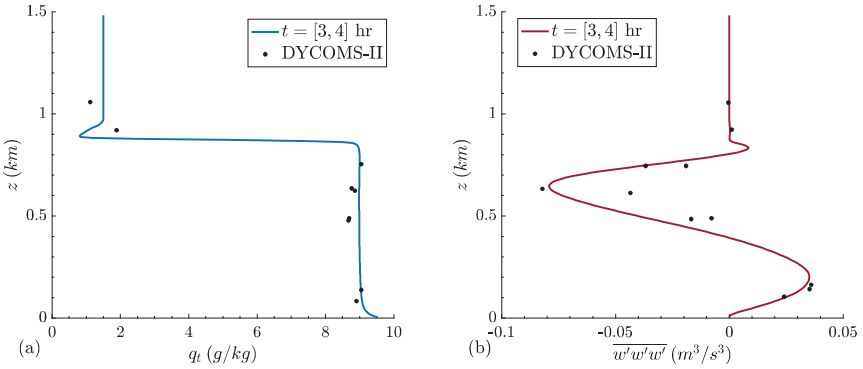

FIGURE 3. Horizontally averaged profiles of (a) total water specific humidity and (b) triple correlation of vertical velocity fluctuations compared against DYCOMS-II field measurements (black dots). The time period denotes the averaging interval which is the same as Stevens *et al.* (2005).

3. Gravity wave model

Atmospheric gravity waves are buoyancy currents whose restoring force is gravity (Mansfield & Sheshadri 2022). These waves have a broad spectrum of horizontal wavelengths and exert significant influence on the large-scale flow by imparting drag and transporting heat upon wave breaking (Alexander & Dunkerton 1999). In a dry, Boussinesq framework with uniform, stable stratification, we can linearize the governing equations and derive a dispersion relation for internal gravity waves

$$\omega^2 = N^2 \cos^2 \theta, \tag{3.1}$$

where ω is the temporal frequency, N is the buoyancy frequency and θ is the angle of the wave vector with respect to the horizontal. Note that Eq. 3.1 allows only four discrete modes of propagation with the constraint of a fixed ω and stratification. This motivates the following model of a gravity wave forcing on the STBL based on the plane wave ansatz that leads to the gravity wave dispersion relation above

$$W_i = Ae^{-(\frac{x-x_c}{a})^2-(\frac{z-z_c}{b})^2} \sin(-\omega t)\delta_{i3}. \tag{3.2}$$

Equation 3.2 is added as a source term to Eq. 2.4, and the effect of the forcing on cloud breakup is investigated. Note that we do not prescribe a wave number as we are interested in perturbing the deck in a localized sense. A denotes the amplitude of the wave; we add a Gaussian centered at $x = x_c$, $z = z_c$ with prescribed widths a and b to ensure seven grid points in both directions across the forcing. The forcing is uniform in y. To validate this model in CM 1, we perform LES with this forcing applied in a stably stratified domain with $\omega = N = 0.01$ s^{-1}. This implies, through Eq. 3.1, that the phase lines be angled at $\theta = 0$. With a choice of $A = 10^{-4}$ m/s^2, Figure 4 illustrates that we recover vertical phase lines with symmetric propagation away from the source and normal to the phase angle.

3.1. *Radiative-convective equilibrium*

To assess any breakup capability of the gravity wave forcing, the STBL needs to achieve a statistically stationary state, i.e. a balance between the dominant heat transfer modes of

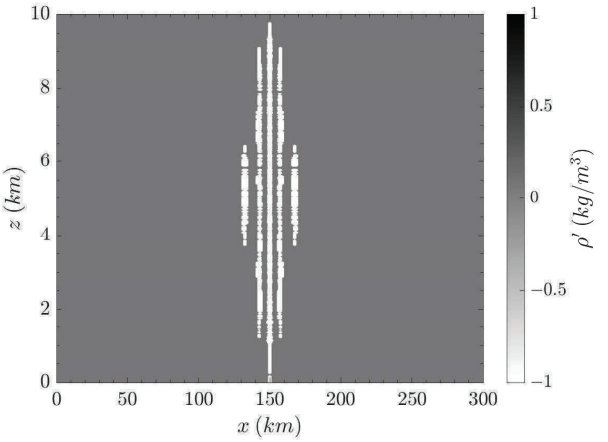

FIGURE 4. Density perturbation contour of the gravity wave forcing (Eq. 3.2) applied in the center of the domain with $\omega = N$.

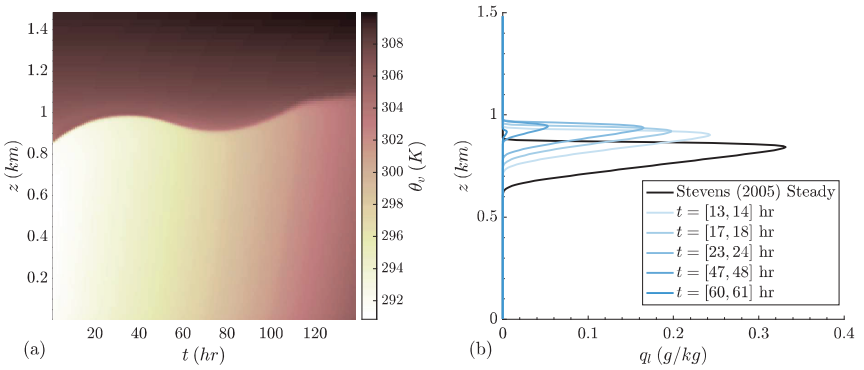

FIGURE 5. a) Spatiotemporal contour of virtual potential temperature and b) liquid water-specific humidity profile through time averaged over the indicated periods. The black line denotes the q_l profile that corresponds to the steady-state time reported by Stevens *et al.* (2005).

convection and radiation. The establishment of radiative-convective equilibrium (RCE) is based on the vertical virtual potential temperature (θ_v) profile attaining stationarity since it is a measure of static stability in a moist environment (Stull 1988). Again, we run the STBL in the manner described in Section 2 but for $t > 3$ hr, which was the reported integration time necessary to reach steady state in Stevens *et al.* (2005). Figure 5(a,b) depicts a Hovmöller diagram of θ_v along with q_l profiles through time.

The boundary layer is statically unstable to begin (Stevens *et al.* 2003), so this initially promotes convective warming near the surface and the observed oscillations of the θ_v near the cloud layer, which corresponds to the adjustment of the cloud top. However, these undulations persist for many days into the simulation, and significant convective warming continues uninhibited. This corresponds to a severe monotonic reduction of the cloud deck, as seen in Figure 5(b), notwithstanding the lack of RCE. The behavior is due to fact that the radiation model (Stevens *et al.* 2005) is insufficient to balance the strong convective activity within the boundary layer. In fact, the radiative fluxes due to cloud-top cooling and cloud-base warming are exponential functions of q_l leading to markedly

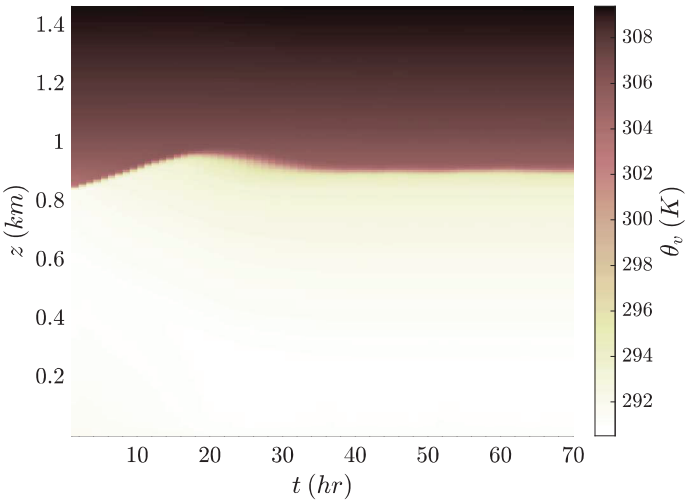

FIGURE 6. Spatiotemporal contour of virtual potential temperature with the updated radiation model of Rotunno & Emanuel (1987).

smaller radiative fluxes imposed through time and thus are unable to counteract the positive feedback of convective heating aiding evaporation. We replaced this radiation model with that of Rotunno & Emanuel (1987) utilizing $t = 1$ hr as a representative large-scale cooling time of the boundary layer (Betts 1986). RCE was achieved at $t = 60$ hr evinced by the θ_v profile changing <1% between successive time stations, as seen in Figure 6.

3.2. *Evaluation of gravity wave model*

Now that we have achieved a statistically stationary profile, the impact of the wave can be investigated. We summarize an initial sweep of STBL simulations varying the following parameters of Eq. 3.2: A, z_c. The forcing is initiated from the RCE state and is active for $t = 1$ hr, representing a time scale of convection within the boundary layer (Betts 1986). As a baseline forcing case, the amplitude and frequency of the wave model are inferred from satellite measurements of mesoscale gravity waves propagating through stratocumulus (Jiang & Wang 2012; Connolly *et al.* 2013). Estimating a time scale of vertical velocity modulation due to the wave as 10^2 s leads to $A = 10^{-4}$ m/s^2 and $\omega = 1.16 \times 10^{-3}$ rad/s. We choose the wave center of the baseline wave as $(x_c, z_c) = (1.6, 0.5)$ km, which is within the stratified cloud layer.

Figure 7 shows the vertical profile of cloud condensate q_c, the portion of q_l neglecting precipitation, through time for the baseline forcing. In the time before forcing, the cloud deck broadens in the vertical as RCE is reached. Upon the forcing period, the stratocumulus maintain their characteristic thickness suggestive of no breakup on the scale of the cloud layer. In other words, the cloud deck is stable to the baseline perturbation as it is unable to further promote any sort of drying mechanism such as entrainment (Bellon & Geoffroy 2016). It is also noted that any background entrainment effects are attenuated since the large-scale radiation model employed does not explicitly include enhanced radiative cooling at the cloud top, which significantly augments dry air entrainment into the STBL.

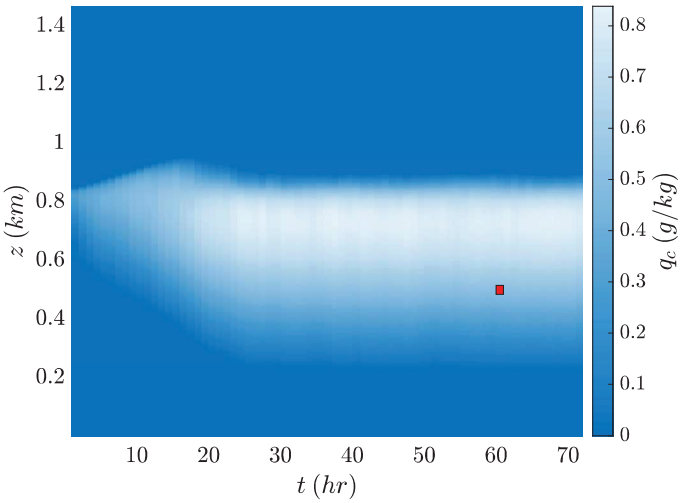

FIGURE 7. Hovmöller diagram of condensate-specific humidity. The red box denotes the spatiotemporal region of the baseline wave forcing.

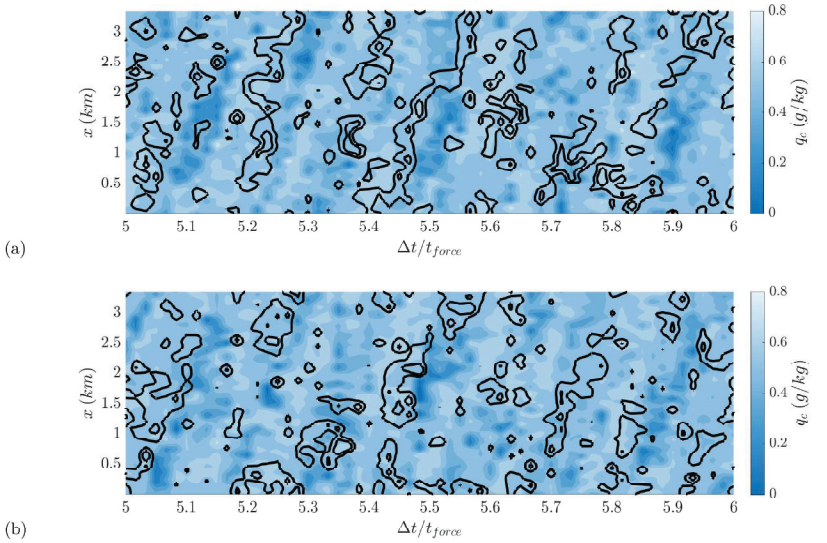

FIGURE 8. Condensate contour at the (y, z) midplane location overlaid with vertical velocity contour lines in black representing $w = [0.5, 2]$ m/s for (a) a forced case with the baseline wave parameters and (b) the control case. The abscissa denotes the time elapsed relative to the forcing duration (t_{force}).

Lastly, we investigated if there was a detectable breakup signature as a result of the baseline forcing. To do so, we fixed our analysis at the midplane with respect to y and z and looked at $q_c(x, t)$ for a case with no wave forcing beyond the defined RCE period (hereafter, control) and one with the baseline forcing. Figure 8(b) seemingly displays coherent periodic transitions between cloudy (high q_c) and clear (low q_c) skies with the

cloudy regions correlated with positive vertical velocity corresponding to upward parcel displacement beyond the lifted condensation level. However, this is not attributable to the forcing (Eq. 3.2), as we observe a similar qualitative oscillation between condensate dense and free areas in the control simulation. This further supports the assertion that the cloud deck is stable to this particular gravity wave model and its effect is no more than slightly modulating the background wave-like disturbances in the stationary state. Similarly, no significant deviation from RCE was observed when the amplitude was increased by an order of magnitude or upon translating the forcing location above the cloud deck (not shown).

4. Discussion and conclusions

Stratocumulus effect change in global scale dynamics through turbulent transport of momentum, heat and moisture between the boundary layer and mesoscale circulation. Their ubiquity across the ocean and land surface make them leading-order contributors to radiative cooling in the overall radiative exchange budget. It is important to understand the regimes that can cause the cloud deck to dissipate, which may have implications for warming under a climate change framework. In this study, we hypothesized that atmospheric gravity waves, which exist across a broadband wavelength spectrum, can lead to breakup of stratocumulus. A spatially localized gravity wave model as a forcing to the vertical momentum equation was implemented once the STBL reached a state of stationarity. It was demonstrated that, in the context of compressible, moist LES, the radiation model utilized in Stevens *et al.* (2005) was incompatible with RCE as a result of the positive feedback between reductions in liquid water and radiative cooling. We establish a robust RCE upon inclusion of a large-scale cooling mechanism. The results of an initial parametric study were presented anchored on a baseline gravity wave forced within the cloud deck with parameters rooted in observational estimates (Jiang & Wang 2012; Connolly *et al.* 2013). Across all runs, it was observed that stratocumulus persist despite sustained forcing, as evident in average cloud profiles and at fixed locations on the grid, which suggest that the gravity wave model posited in this study establishes a starting lower bound in wave amplitude to elicit a breakup response.

Future work will include investigating a stronger amplitude in tandem with a larger forcing region. In addition, we plan to explicitly model radiative sources, such as shortwave and longwave effects, along with representing mesoscale cloud systems via increasing domain extent, all of which will further our understanding of stratocumulus.

Acknowledgments

A.B. acknowledges support from a National Science Foundation Graduate Research Fellowship (Grant Number DGE-1656518). The authors acknowledge computing resources provided by the Stanford Research and Computing Center.

REFERENCES

Alexander, M. J. & Dunkerton, T. J. 1999 A spectral parameterization of mean-flow forcing due to breaking gravity waves. *J. Atmos. Sci.* **56**, 4167–4182.

Bellon, G. & Geoffroy, O. 2016 Stratocumulus radiative effect, multiple equilibria of the well-mixed boundary layer and transition to shallow convection. *Q. J. Roy. Meteor. Soc.* **142**, 1685–1696.

Betts, A. K. 1986 A new convective adjustment scheme. Part I: observational and theoretical basis. *Q. J. Roy. Meteor. Soc.* **112**, 677–691.

Bryan, G. H. & Fritsch, M. J. 2002 A benchmark simulation for moist nonhydrostatic numerical models. *Mon. Weather Rev.* **130**, 2917–2928.

Connolly, P. J., Vaughan, G., Cook, P., Allen, G., Coe, H., Choularton, T. W., Dearden, C. & Hill, A. 2013 Modelling the effects of gravity waves on stratocumulus clouds observed during VOCALS-UK. *Atmos. Chem. Phys.* **13**, 7133–7152.

Deardorff, J. W. 1980 Stratocumulus-capped mixed layers derived from a three-dimensional model. *Boundary-Layer Meteorol.* **18**, 495–527.

Jiang, Q. & Wang, S. 2012 Impact of gravity waves on marine stratocumulus variability. *J. Atmos. Sci.* **69**, 3633–3651.

Klemp, J. B., & Wilhelmson, R. B. 1978 The simulation of three-dimensional convective storm dynamics. *J. Atmos. Sci.* **35**, 1070–1096.

Mansfield, L. A., & Sheshadri, A. 2022 Calibration and uncertainty quantification of a gravity wave parameterization: a case study of the Quasi-Biennial Oscillation in an intermediate complexity climate model. *J. Adv. Model. Earth Sy.* **14**, e2022MS003245.

Mellado, J. P. 2017 Stratocumulus clouds *Annu. Rev. Fluid Mech.* **49**, 145–169.

Morrison, H., Curry, J. A., & Khvorostyanov, V. I. 2005 A new double-moment microphysics parameterization for application in cloud and climate models. Part I: description *J. Atmos. Sci.* **62**, 1665–1677.

Pressel, K. G., Mishra, S., Schneider, T., Kaul, C. M., & Tan, Z. 2017 Numerics and subgrid-scale modeling in large eddy simulations of stratocumulus clouds. *J. Adv. Model. Earth Sy.* **9**, 1342–1365.

Randall, D. A., Coakley, J. A., Fairall, C. W., Knopfli, R. A., & Lenshow, D. H. 1984 Outlook for research on marine subtropical stratocumulus clouds. *B. Am. Meteorol. Soc.* **65**, 1290–1301.

Rotunno, R., & Emanuel, K. A. 1987 An air–sea interaction theory for tropical cyclones. Part II: evolutionary study using a nonhydrostatic axisymmetric numerical model. *J. Atmos. Sci.* **44**, 542–561.

Schneider, T., Kaul, C., & Pressel, K. 2019 Possible climate transitions from breakup of stratocumulus decks under greenhouse warming. *Nature* **12**, 163–167.

Slingo, A. 1990 Sensitivity of the Earth's radiation budget to changes in low clouds. *Nature* **343**, 49–51.

Stevens, B., Lenschow, D. H., Vali, G., Gerber, H., Bandy, A., Blomquist, B., Brenguier, J. L., Bretherton, C. S., Burnet, F., Campos, T. *et al.* 2003 Dynamics and chemistry of marine stratocumulus–DYCOMS-II *B. Am. Meteorol. Soc.* **84**, 579–594.

Stevens, B., Moeng, C. H., Ackerman, A. S., Bretherton, C. S., Chlond, A., De Roode, S., Edwards, J., Golaz, J., Jiang, H., Khairoutdinov, M. *et al.* 2005 Evaluation of large-eddy simulations via observations of nocturnal marine stratocumulus. *Mon. Weather Rev.* **133**, 1433–1462.

Stull, R. B. 1988 *An Introduction to Boundary Layer Meteorology.* Springer Science & Business Media.

Wood, R. 2012 Stratocumulus clouds *Mon. Weather Rev.* **140**, 2373–2423.